-RESEARCH PAPER-

International Journal of Mining and Geo-Engineering

IJMGE

IJMGE 59-3 (2025) 255-265

DOI: 10.22059/IJMGE.2025.381819.595192

Modelling of soils using isotropic and anisotropic models

Behnam Ghobadi [a], Ehsan Taheri [a, *], Seyed Ali Ghoreishian Amiri [b] and Mosleh Eftekhari [a]

[a] *Faculty of Engineering, Tarbiat Modares University, Tehran, Iran.*

[b] *PoreLab, Department of Civil and Environmental Eng., Norwegian University of Science and Technology (NTNU), Trondheim, Norway.*

Article History:

Received: 03 September 2024.

Revised: 14 May 2025.

Accepted: 08 July 2025.

ABSTRACT

In this study, two behavioral models—unified and multilaminate—are employed to simulate soil behavior. The unified model incorporates a non-associated flow rule along with the critical state concept. Additionally, the sub-loading surface concept is adopted to capture a smooth elastic-plastic transition. For numerical implementation, the implicit Euler method is used**.** The multilaminate model is based on a 13-plane framework, in which each plane exhibits elastic-plastic behavior. The overall soil response is obtained by integrating the elastic-plastic responses of the individual planes oriented in various directions at a material point. A set of unconventional constitutive equations is applied to each plane. This model captures soil softening behavior more realistically due to the use of a non-classical plasticity approach. Moreover, it accounts for the effect of induced anisotropy**.** To evaluate the models, four clay samples subjected to monotonic loading—under both drained and undrained conditions—were analyzed using both the unified and multilaminate models and were compared with experimental data. The results demonstrate that the unified model offers a more favorable representation of soil behavior.

Keywords: *General dilatancy rule, Implicit method, Multilaminate theory, Sub-loading surface, Unified model.*

1. Introduction

During recent decades, various constitutive models have been presented to model the behavior of clay and sand. In this regard, based on the critical state concept, the Cam-Clay model (CCM) was presented by Roscoe and Schofield [1]. This model has been successful in simulating the behavior of normally consolidated clay [2]-[4]. Subsequently, maintaining the same methodological framework, Roscoe and Burland (1968) proposed the modified Cam-Clay (MCC) model specifically for clay exhibiting a higher overconsolidation ratio [5]. However, the proposed models have limitations in simulating the behavior of overconsolidated clay and sand (Fig. 1). These limitations include the overprediction of yield stress due to the yield surface used in these models for overconsolidated clay [4], [6]. Indeed, using the associated flow rule in the mentioned models results in poor predictions of behavioral characteristics, such as those of normally consolidated clay under undrained conditions (Fig. 2) conditions [7], [8]. Furthermore, the CCM and MCC version were not developed for sand [8]-[11]. In this context, numerous modifications have been made to these models to achieve accurate predictions of the behavior of overconsolidated clay and sand [3], [12]-[17]. However, the proposed models are only suitable for predicting the behavior of either clay or sand. As a result, further efforts were made to develop unified behavioral models. Yu (1998) proposed a unified model for both clay and sand, known as the CASM [18]. In this model, a unified yield function and the concepts of critical state and state parameter are used. The unified CASM model follows a non-associated flow rule. Yu demonstrated that the proposed model can effectively predict the behavior of both clay and sand within a unified framework. However, the CASM model followed the classical plasticity theory, which led to the prediction of sudden behavior from the elastic to the plastic state. This model was not able to model the smooth behavior observed in real soil behavior. Therefore, Yu and Khong (2003) introduced the CASM-b model, which utilizes the concept of a bounding surface [19]. Their proposed model can predict a smooth behavior from the elastic to the plastic state. However, an explicit numerical integration method has been used in the presented models. According to the conducted research, it has been demonstrated that the use of explicit numerical integration methods in the implementation of behavioral models leads to convergence for small strains; however, the solutions do not converge for large strains. Conversely, it has been shown that the use of implicit numerical integration methods in the implementation of behavioral models can result in the convergence of responses for each increase in strain. [13],[20]-[23]. Moghadam et al. proposed a new formulation based on the concept of the bounding surface and on using the implicit method to model the behavior of overconsolidated clay [24]. This model can predict the behavior of overconsolidated smooth clay with proper accuracy and convergence. Recent advancements in unified models have demonstrated their efficacy in simulating the behavior of both clay and sand. However, these models exhibit limitations when it comes to accurately predicting the phase transition behavior that is commonly observed in overconsolidated clay and dense sand. This is due to the dilatancy rule considered in these models. According to the research conducted in this field, it has been determined that soil dilatancy depends on the state parameter in addition to the stress ratio [12], [25]. While the dilatancy rule incorporated in the CASM model is solely dependent on the stress ratio. Therefore, in the present model, a general dilatancy rule is employed, which depends on the state parameter and internal variables of the soil. In this study, we present a unified model that characterizes the behavior of clay and sand under monotonic loading conditions, both drained and undrained. The proposed model utilizes the concept of a bounding surface, based on the radial mapping rule, to effectively simulate smooth behavior. This model is presented in the form of the critical state and state parameter concepts. Additionally, the proposed

* Corresponding author: *E-mail address:* e_taheri@modares.ac.ir (E. Taheri).

unified model incorporates a non-associated flow rule along with an isotropic hardening rule. Furthermore, an implicit method based on the return mapping algorithm has been employed to implement the current model.

In this research, the code of Moghadam et al. (2022) has been developed. To verify the developed code, the results from triaxial tests were utilized. In the literature, a considerable number of triaxial tests have been presented to investigate the behavior of soils under monotonic and cyclic loading, for drained and undrained conditions [26]-[31]. Several of these tests were selected to verify the model. Subsequently, the results of the unified behavioral model have been compared with those of the multilaminate behavioral model and laboratory data. The unified model shows a more acceptable performance in modelling soil behavior under monotonic loading in both drained and undrained conditions. The unified model accurately predicts the behavioral characteristics of clay and sand under monotonic loading, including soft behavior, transitioning from elastic to plastic, softening and hardening behaviors, dilatancy, and phase transition behavior.

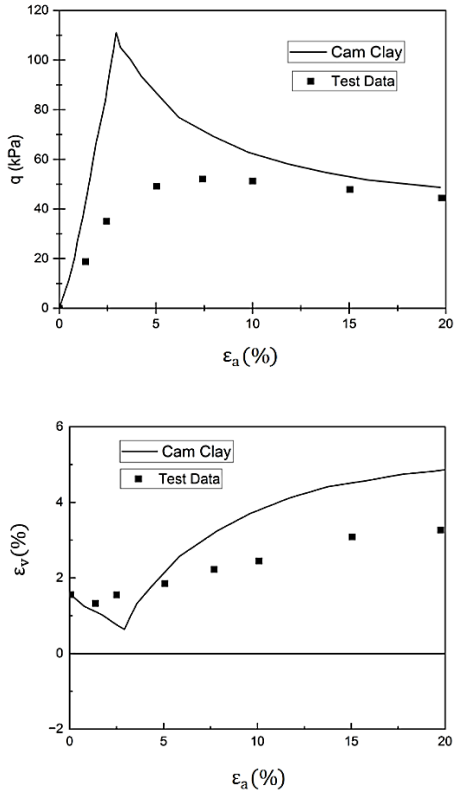

Figure 1. Cam- Clay prediction for drained compression of a heavily over consolidated of Weald clay (OCR=24).

1.1. Innovations of the article

In the following article, a unified behavioral model is utilized to model the behavior of clay and sand. Additionally, the non-associate flow rule is used. A general flow rule for clay and sand has also been employed, which effectively models the behavior of overconsolidated clays. Furthermore, the results of the unified behavioral model are compared with those of the multilaminate behavioral model.

2. Description of the unified model

In this section, the proposed unified model for clay and sand to model the monotonic loading behavior under drained and undrained conditions is presented in detail. The bounding surface theory is employed based on a radial mapping rule. This model incorporates the concepts of the critical state and state parameter to provide a unified representation of clay and sand behavior. To determine the plastic strain in the current model, the non-associated flow rule is utilized. Moreover, to establish a relationship between the increase in plastic volumetric strain and the increase in plastic deviatoric strain, a general dilatancy rule has been incorporated into this model. Additionally, to implement the model, an implicit numerical integration method based on the return mapping algorithm has been employed. The elastic-plastic equations used in the proposed model, based on the implicit method, are given in section 3.

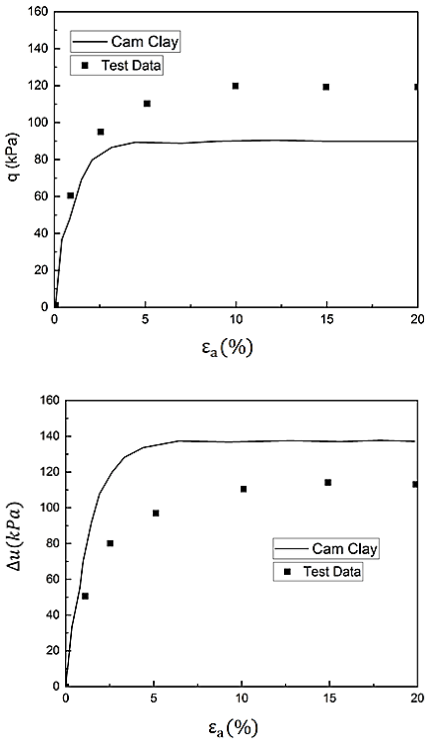

Figure 2. Cam- Clay prediction for undrained compression of a normally consolidated of weald clay (OCR=1)

2.1. General formulation of the model

To describe the behavior of the soil under triaxial stress conditions, the components of the average effective stress p' and the deviatoric stress q have been utilized, as defined by the following relationships [32].

$$p' = \frac{\sigma_1+\sigma_2+\sigma_3}{3} \quad (1)$$

$$q = \frac{1}{\sqrt{2}}\sqrt{(\sigma_1-\sigma_2)^2+(\sigma_1-\sigma_3)^2+(\sigma_2-\sigma_3)^2} \quad (2)$$

Furthermore, the volumetric strains ε_V and deviatoric ε_q corresponding to the stress components are expressed according to the following relationships:

$$\varepsilon_V = \varepsilon_1 + \varepsilon_2 + \varepsilon_3 \quad (3)$$

$$\varepsilon_q = \frac{2}{3}(\varepsilon_1 - \varepsilon_3) \quad (4)$$

Additionally, based on the plasticity theory, it is assumed that the increase in total strain $d\varepsilon$ consists of two components: elastic and plastic, as expressed in Equation (5):

$$d\boldsymbol{\varepsilon} = d\boldsymbol{\varepsilon}^e + d\boldsymbol{\varepsilon}^p \quad (5)$$

In this context, $d\boldsymbol{\varepsilon}^e$ represents the increment of elastic strain, which can be determined using the elastic behavior parameters of the soil

discussed in section 2.4.

In the above relationship, $d\boldsymbol{\varepsilon}^p$ represents the increase in plastic strain, which is calculated based on the non-associated flow rule and the concept of the bounding surface (see Sections 2.10 and 2.12). In the current model, compression loading is considered positive and tension loading is considered negative for deviatoric stress.

2.2. Critical state

The critical state of soil refers to a specific condition in soil mechanics where the soil reaches a state of constant volume and constant shear stress during shearing. In the current model, the critical state is defined by a line in the $e - lnp'$ and $q - p'$ planes. The critical state void ratio is related to the confining pressure, and its value decreases as the confining pressure increases. The critical state line (CSL) is defined in the $e - lnp'$ and $q - p'$ planes by the following Equations [32]:

$$e_{\mathrm{cr}} = e_{\Gamma} - \lambda_{\mathrm{cr}} lnp' \tag{6}$$

$$q = M_{\mathrm{cr}} p' \tag{7}$$

In this context, e_{cr} represents the critical state void ratio. To establish the critical state line in the $e - lnp'$ plane, two parameters, e_Γ and λ_{cr}, are utilized. These parameters represent the critical state void ratio corresponding to $p' = 1kPa$ and the slope of the critical state line in this plane, respectively.

As shown in Figure 3, the critical state line in the $q - p'$ plane is determined by a straight line with slope M_{cr} passing through the origin of the graph. In this context, M_{cr} is calculated using the Mohr-Coulomb criterion in the yield state, based on the soil internal friction angle φ [33]:

$$M_{\mathrm{cr}} = \frac{6sin\varphi}{3t - sin\varphi} \tag{8}$$

The Equation defines t as a scalar parameter that depends on the type of loading. In the case of compressive loading, $t = +1$ and $M_{\mathrm{cr}} = M_{\mathrm{c}}$; whereas for tensile loading, $t = -1$ and $M_{\mathrm{cr}} = M_{\mathrm{e}}$ are considered.

2.3. State parameter

The state parameter in soil mechanics is a concept used to describe the current condition of a soil element in terms of its stress and volumetric characteristics. It is particularly useful in understanding the behavior of soils under different loading conditions. In the current model, the state parameter is determined according to the following relationship [8]:

$$\psi = \vartheta - \vartheta_{cr} = \vartheta - (\vartheta_{\Gamma} - \lambda \ln(p')) \tag{9}$$

where ϑ_Γ and λ are material parameters that define the critical state line in the $\vartheta - \ln(p')$ plane.

2.4. Elastic behavior

In the proposed model, the elastic behavior of soil is described by the bulk modulus K and shear modulus G [34].

$$\mathrm{K} = \frac{\nu p'}{\kappa} \tag{10}$$

$$\mathrm{G} = \frac{3(1-2\mu)}{2(1+\mu)}\mathrm{K} \tag{11}$$

In these relationships, $\nu = 1 + e$ is the specific volume, κ is the slope of the loading-unloading line in the $e - lnp'$ plane, and μ denotes the Poisson's ratio.

2.5. Plastic behavior

The models presented based on the classical plastic theory are based on the assumption that the inner region of the yield surface is completely elastic [32], [35]. As a result, considering this assumption in such models makes the behavior of the material completely elastic until the stress state reaches the yield point, and then the behavior of the material changes to an elastic-plastic state. Therefore, such an assumption will lead to the prediction of a sudden behavior from elastic to plastic state. However, according to laboratory observations, it has been determined that materials under loading show a soft behavior [32], [35]. In this context, to predict the soft behavior of materials, the non-classical plastic theory based on the bounding surface concept by Dafalias and Popov [36], along with the subloading surface theory by Hashiguchi [37],[38], has been introduced. In the current model, the bounding surface theory has been employed to describe plastic behavior, owing to its relative simplicity and ease of implementation.

According to the bounding surface theory, plastic deformations are created from the beginning of loading and the elastic area is reduced to one point [14], [39]-[40]. This theory uses two internal and external surfaces to describe elastic-plastic behavior [36], [39]-[41], in which the inner surface is considered as the loading surface and the current stress point always passes through it. According to this theory, the external surface is considered as the bounding surface and the image stress state is always placed on this surface. Various models have been developed to predict the cyclic and monotonic responses of soils based on these approaches [42]-[45]. The use of two loading surfaces, the loading surface and the bounding surface according to this theory is shown in Figure 3.

To determine the image stress state corresponding to the current stress state, a mapping rule is utilized [39], [41].

2.6. Radial mapping rule

As shown in figure 3, in the current model, a radial mapping rule is used to determine the image of the current stress state on the bounding surface. Based on the radial mapping rule, the image of the stress point on the bounding surface, defined by a straight line that passes through the origin of the stress space and the current stress point on the loading surface, determines the image of the stress on the bounding surface [14], [39], [41].

According to the geometric similarity of loading and bounding surfaces, the following relationship can be established between the current state of stress and its image, as well as the stress components:

$$\gamma = \frac{\boldsymbol{\sigma}}{\boldsymbol{\sigma}_j} = \frac{q}{q_j} = \frac{p'}{p'_j} = \frac{p'_c}{p'_{cj}} \tag{12}$$

In this Equation, γ is defined as the ratio of the size of the surfaces and determines the distance or proximity of the loading surface to the bounding surface. In the above relationship, $\boldsymbol{\sigma}$ specifies the current stress state, p' is the average effective stress component, and q is the deviatoric stress component related to the current stress state. In addition, $\boldsymbol{\sigma}_j$ expresses the image stress state on the bounding surface, p'_j is the average effective stress component and q_j is the deviatoric stress component corresponding to the image stress state. Also, p'_c controls the size of the loading surface and p'_{cj} is the isotropic hardening parameter that determines the size of the bounding surface.

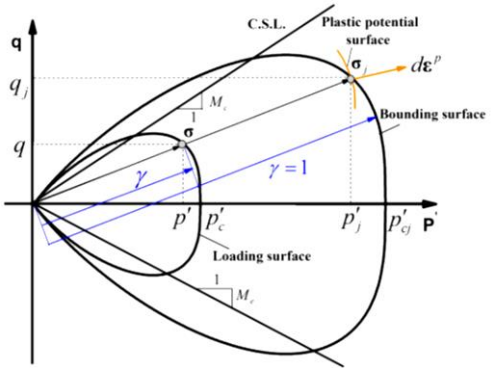

Figure 3. Loading surface, bounding surface and radial mapping rule according to the bounding surface theory

2.7. Loading surface

To describe the unified behavior of clay and sand, the yield function proposed by Yu has been utilized in the current model. Here, the loading surface function is defined according to the following Equation [18].

$$F(\boldsymbol{\sigma}) = \left(\frac{q}{M_{cr}p'}\right)^N + \ln\left(\frac{p'}{p'_c}\right)/\ln(R) \quad (13)$$

Where N and R are the material parameters. The parameter N controls the shape of the loading surface and the parameter R expresses the ratio between the values of p'_c and p' at the intersection point of the yield surface and the critical state line.

In addition, the value of M_{cr} according to Equation (8), is dependent on the type of loading, where:

$$\begin{cases} if\ q > 0\ then\ t = +1, \text{compressive loading} \\ if\ q \le 0\ then\ t = -1, \text{extensive loading} \end{cases} \quad (14)$$

2.8. Bounding surface

According to the bounding surface theory, in the present model, it is assumed that the bounding surface has the same shape as the loading surface. The bounding surface function in the proposed model is defined according to the following relationship:

$$F(\boldsymbol{\sigma}_j) = \left(\frac{q_j}{M_{cr}p'_j}\right)^N + \ln\left(\frac{p'_j}{p'_{cj}}\right)/\ln(R) \quad (15)$$

2.9. General dilatancy rule and plastic potential function

The dilatancy rule dictates the orientation of plastic flow within materials [25], [46]. In this study, the general dilatancy rule proposed by Li and Dafalias has been slightly modified to account for the effects of the overconsolidation ratio (OCR), specifically for clay materials.

$$\frac{d\varepsilon_v^p}{d\varepsilon_q^p} = \frac{d_0}{M_{cr}}\left(\frac{M_{cr}}{\bar{\eta}}\gamma^\beta \exp(m\psi) - 1\right) \quad (16)$$

In this Equation, d represents the dilatancy, $d\boldsymbol{\varepsilon}_v^p$ is the increase in the plastic volumetric strain, $d\boldsymbol{\varepsilon}_q^p$ is the increase in the plastic deviatoric strain, d_0, m and β are the parameters of the material and $\bar{\eta}$ is the stress ratio. This relationship can well model the behavior of both clay and sand. In the proposed model, the direction of the plastic strain vector is determined by the vector perpendicular to the plastic potential surface. The function of the plastic potential surface is obtained by integrating Equation (16):

$$Q(\boldsymbol{\sigma}) = \frac{q}{p'} + \frac{d_0 e^{\beta\psi}}{1-\frac{d_0}{M_{cr}}}\left[1 - \left(\frac{p'_0}{p'}\right)^{1-\frac{d_0}{M_{cr}}}\right] \quad (17)$$

Where p'_0 determines the size of the plastic potential surface. However, this variable has no effect on the calculations of the plastic strain and is removed from the calculations by deriving the relation for the plastic potential function.

2.10. Non - associated flow rule

To determine the size and direction of plastic strains in the current model, a non-associated flow rule has been employed [32].

$$d\boldsymbol{\varepsilon}^p = \frac{d\lambda\frac{\partial Q}{\partial \sigma}}{\left\|\frac{\partial Q}{\partial \sigma}\right\|} = d\lambda.\boldsymbol{m} \quad (18)$$

Where $\boldsymbol{m} = \frac{\partial Q}{\partial \sigma}/\left\|\frac{\partial Q}{\partial \boldsymbol{\sigma}}\right\|$ specifies the unit vector that is perpendicular to the plastic potential surface and the direction of the plastic strain vector is determined by this vector. Also, $d\lambda$ is the plastic coefficient and the size of the plastic strain increase is determined by it ($\|d\boldsymbol{\varepsilon}^p\| = d\lambda$). In addition, the volumetric and deviatoric components of the plastic strain increase vector can be calculated by the following relations:

$$d\boldsymbol{\varepsilon}_v^p = d\lambda\frac{\partial Q}{\partial p'}/\left\|\frac{\partial Q}{\partial \boldsymbol{\sigma}}\right\| = d\lambda.m_p \quad (19)$$

$$d\boldsymbol{\varepsilon}_q^p = d\lambda\frac{\partial Q}{\partial q}/\left\|\frac{\partial Q}{\partial \boldsymbol{\sigma}}\right\| = d\lambda.m_q \quad (20)$$

Where $m_p = \frac{\frac{\partial Q}{\partial p'}}{\left\|\frac{\partial Q}{\partial \sigma}\right\|}$ and $m_q = \frac{\partial Q}{\partial q}/\left\|\frac{\partial Q}{\partial \boldsymbol{\sigma}}\right\|$ are respectively the volumetric and deviatoric components of the unit vector perpendicular to the plastic potential surface. In Figure 4, the application of the non-associated flow rule is shown.

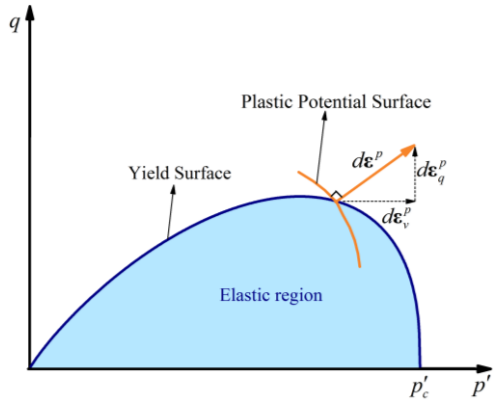

Figure 4. Non - associated flow rule.

In this context, the dilatancy relation can be employed to calculate the increase in the plastic strain vector and its components. Considering that the size of the vector m is equal to one, $\|\boldsymbol{m}\| = \sqrt{m_p^2 + m_q^2} = 1$, and also using the dilatancy relation $d = \frac{d\varepsilon_v^p}{d\varepsilon_q^p} = \frac{m_p}{m_q}$, we will have:

$$d\boldsymbol{\varepsilon}_v^p = \frac{d}{\sqrt{1+d^2}} \quad (21)$$

$$d\boldsymbol{\varepsilon}_q^p = \frac{t}{\sqrt{1+d^2}} \quad (22)$$

2.11. Isotropic hardening rule

Based on the isotropic hardening rule, by creating plastic deformations, the yield surface can expand or contract in the stress space while keeping the shape and location constant (Figure 5). According to the hardening rule considered in the present model, the changes in the size of the bounding surface dp'_{cj} will be linearly related to the increase in the plastic volumetric strain $d\varepsilon_v^p$ [34].

$$dp'_{cj} = p'_{cj}\frac{\vartheta}{\lambda-\kappa}d\boldsymbol{\varepsilon}_v{}^p \quad (23)$$

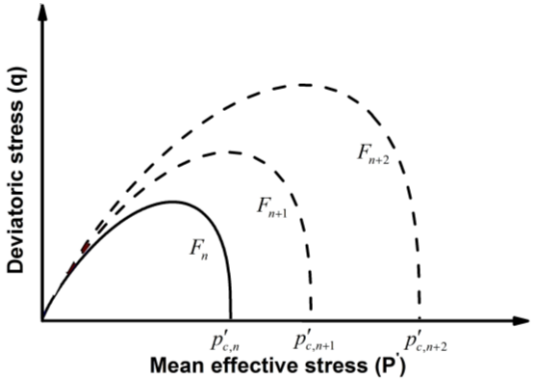

Figure 5. Isotropic hardening rule.

2.12. The rule governing changes in the ratio of surface sizes

To facilitate plastic deformations from the onset of loading, the proposed model assumes that plastic strains vary according to the size ratio of the loading surface to the bounding surface. To achieve this, a rule is applied to account for changes in the surface size ratio, as

described by the following Equation [35].

$$d\gamma = U(\gamma) \parallel d\boldsymbol{\varepsilon}^p \parallel, \parallel d\boldsymbol{\varepsilon}^p \parallel = d\lambda \tag{24}$$

In this Equation, U(γ) is a decreasing function of γ that must satisfy the following conditions [40].

$$\begin{aligned} &U(\gamma) = +\infty \; for \; \gamma = 0 \\ &U(\gamma) > 0 \; for \; 0 < \gamma < 1 \\ &U(\gamma) = 0 \; for \; \gamma = 1 \\ &U(\gamma) < 0 \; for \; \gamma > 1 \end{aligned} \tag{25}$$

Thus, the function provided by Hashiguchi [35] was utilized to establish the conditions outlined in Equation 25.

$$U(\gamma) = -uln(\gamma) \tag{26}$$

Equation (26) correctly establishes the conditions of Equation (25). In this Equation, u is the material parameter.

3. Implementation of the model by implicit method

In this section, the implementation of the proposed model is presented in an implicit way, based on the return mapping algorithm. Unlike the return mapping algorithm in classical models, which necessitates a process to ascertain whether the stress state lies outside or inside the yield surface, the algorithm employed in this model simplifies the elastic state to a single point. Consequently, it does not involve a state determination process. The process related to the implementation algorithm of the proposed model includes two steps: predicting the elastic state and correcting the plastic state.

3.1. The process of predicting the elastic state

In the elastic state prediction process, at each loading step, the stress state is calculated, assuming that the strains are elastic:

$$\boldsymbol{\sigma}^{Trial} = \boldsymbol{\sigma}_n + \boldsymbol{D}^e_{n+1} d\boldsymbol{\varepsilon}_{n+1} \tag{27}$$

In this Equation, $\boldsymbol{\sigma}^{Trial}$ specifies the stress on the elastic state, n and $n+1$ represent the previous step and the current step, respectively, and $\boldsymbol{D}^e$ is the material's elastic matrix. During the continuation of the process, the elastic state stress and other state variables are adjusted in the plastic correction process. Figure 6 illustrates the changes in the yield surface due to plastic deformation, in accordance with the isotropic hardening rule.

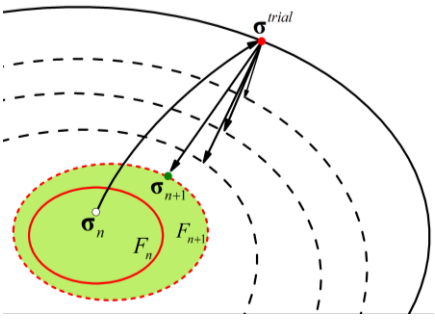

Figure 6. Return mapping algorithm.

It should be noted that the return mapping algorithm here means that in each loading step, the elastic stress state is returned to the current loading surface by the elastic-plastic equations. The calculation method based on this algorithm is shown in Figure 6.

3.2. Plastic correction process

During this process, the amount of elastic stress calculated in the previous process, the flow rule, the isotropic hardening rule, as well as the changes in the ratio of surface sizes rule, will be corrected in such a way that the consistency condition is established. Thus, to establish the specified conditions, the following equations were employed in the plastic correction process.

a. Equilibrium equation

The state of stress should always satisfy the equilibrium Equation:

$$d\boldsymbol{\sigma} = \boldsymbol{D}^e d\boldsymbol{\varepsilon}^e \tag{28}$$

By implicitly integrating the above Equation from step n to n+1 and also inserting relations (5) and (27) into the resulting Equation, the equilibrium Equation is obtained according to the following Equation.

$$\boldsymbol{\sigma}_{n+1} = \boldsymbol{\sigma}^{Trial} - \boldsymbol{D}^e_{n+1} d\boldsymbol{\varepsilon}_{n+1}{}^p \tag{29}$$

b.Surface size ratio changes

To generate plastic strains based on the size ratio of the surfaces, Equation (24) must be established. Therefore, by numerically implicitly integrating this Equation, we will have:

$$\gamma_{n+1} = \gamma_n - uln(\gamma_{n+1}) d\lambda \tag{30}$$

c. Isotropic hardening rule

By creating plastic deformations, the bounding surface expands or contracts according to the isotropic hardening rule. Therefore, by numerical implicit integration of Equation (23), the following relationship is obtained:

$$p'_{cj,n+1} = p'_{cj,n} \exp\left(\frac{\vartheta_n}{\lambda-\kappa}(d\boldsymbol{\varepsilon}_v{}^p)_{n+1}\right) \tag{31}$$

d. Consistency condition

Based on the consistency condition, the stress state should always be located on the loading surface in elastic-plastic conditions [35]. Therefore, the current stress state must satisfy the loading surface Equation:

$$F(\boldsymbol{\sigma}_{n+1}) = \left(\frac{q_{n+1}}{M_{cr} p'_{n+1}}\right)^N + \frac{\ln\left(\frac{p'_{n+1}}{\gamma_{n+1} p'_{cj,n+1}}\right)}{\ln(R)} = 0 \tag{32}$$

Finally, by establishing Equations (29)-(32) at the same time, a system of nonlinear equations is formed. To solve this system of Equations, the Newton-Raphson iterative procedure is used. In Fig. 7, the unified model algorithm is presented in an implicit format.

4. Calculation of model input parameters

The unified model comprises 12 input parameters for monotonic loading, and the values of these parameters must be measured prior to modelling. In this model, the elastic behavior of the soil is defined by μ and κ. The Poisson's ratio μ affects the shear modulus and for soil it has a value between 0.2 and 0.4 and can be determined by the triaxial test considering the elastic behavior in the plane $\varepsilon_a - \varepsilon_v$ [32], [47]. κ expresses the slope of the unloading line in the $\vartheta - lnp'$ plane. This parameter has a value between 0.001 and 0.01 for sand and 0.01 and 0.06 for clay [32], and its value can be determined by isotropic consolidation tests. In the proposed model, $M_{cr}, \lambda, e_\Gamma$ are critical state parameters. λ, e_Γ determines the position of the critical state line in the $e - \ln(p')$ plane. λ represents the slope of the critical state line (loading line) and e_Γ specifies the critical state void ratio at unit confining pressure and can be obtained using isotropic consolidation tests. In addition, M_{cr} expresses the slope of the critical state line in the $q - p'$ plane and has different values for the compressive and extensive loading states, which are indirectly determined based on the internal friction angle in the yielding state of the soil. Also, this parameter can be determined directly using triaxial tests by the ratio of critical state effective stresses in different loading paths. In the present model, as in the model presented by Yu, two parameters N and R are used in the yield function equation, where N controls the shape of the yield surface and R determines the ratio between p'_c and p' at the point where the critical state line

intersects the loading surface. These parameters are assumed to be constant in the Cam-Clay and MCC models. For the values of $N = 1$ and $R = 2.718$, the yield surface of the CCM is obtained, and for the values of $N = 1.7$ and $R = 2$, the yield surface of the modified Cam-Clay model is approximately obtained. According to the laboratory results, the value of R for clay is in the range of 1.5 to 3 and for sand it has larger values. Also, the parameter N has a value between 1 and 5 [32]. The values of N and R can be calibrated by effective stress paths obtained from undrained triaxial tests on soils in their loose state. Under the assumption that elastic strains are negligible compared to plastic strains, the dilatancy parameters (d_0 , β ,m) can be determined by fitting the stress-ratio-total dilatancy curve in standard drained triaxial compression tests. The parameter u is introduced in this model based on bounding surface theory, which controls the transition from elastic to plastic behavior in materials. It can be determined from the stress-strain curve; smaller values of u indicate softer material behavior, while larger values lead to a sudden shift towards classical behavior.

5. Multilaminate model

In the multilaminate framework, the core approach involves calculating the numerical integral of a specific mathematical function by expanding it on the surface of a unit sphere. This function represents variations in various physical properties across the sphere's surface [48]-[52]. In this research, a model consisting of 13 planes, each exhibiting elastic-plastic behavior, was utilized to estimate the sphere's surface. The overall behavior of the soil is derived from the cumulative effects of these planes. Each plane is described by a series of non-classical structural equations. To evaluate the function values at each point, a well-known relation is employed based on the function values from the different planes of the hemisphere.

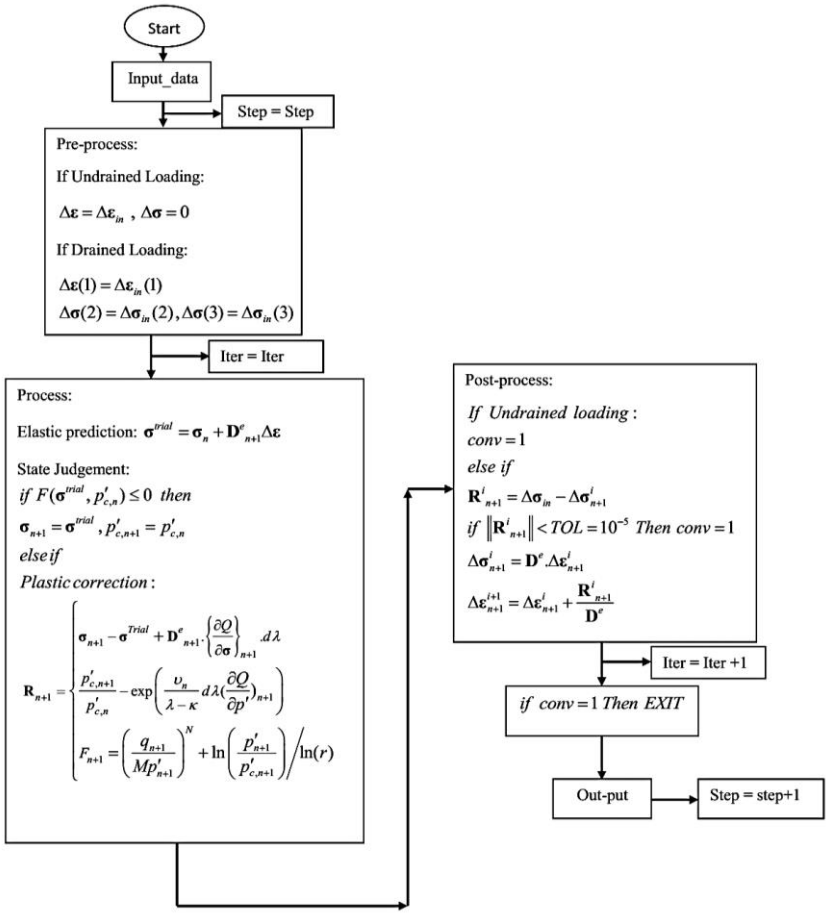

Figure 7. Unified model program algorithm using the implicit method.

$$\int_{\Omega}\int f(x,y,z)d\Omega = 8\pi\sum_{i=1}^{i=13} w_i f_i\,(x_i, y_i, z_i) \tag{33}$$

Ω shows the area of the sphere. n represents the number of defined points and w_i is the weight coefficient of the i-th base point. The position of the sphere and the 26 defined points are shown in Figure 8.

The direction cosines of the desired 13 planes along with their weight coefficients are shown in Table 1, and the extension of the 13 planes in the center of the cube is shown in Figure 9.

This program is able to model the soil softening behavior more realistically due to the use of a non-classical plasticity model. In fact, it somehow considers the effect of induced anisotropy. The multi-plane model has six parameters that must be calibrated through laboratory test data. These parameters are: λ, M_{cr}, κ, u_0, μ and F_0. The calculation method of these parameters was presented in the previous section. A hardening-softening function has been used for soil in the form of the following relationship [53], [54].

$$F = F_0 \exp\left(\frac{H}{\lambda-\kappa}\right) \tag{34}$$

In this formula, parameter F_0 represents the initial value of F. In classical continuum mechanics, it is common to describe the evolution of the isotropic hardening/softening variable by volumetric plastic strain. Therefore, the isotropic hardening/softening variable in this model is related to plastic strain, which plays the role of volumetric plastic strain in the multi-plane model, in its simplest form.

$$\dot{H} = \dot{\varepsilon}^p_n \tag{35}$$

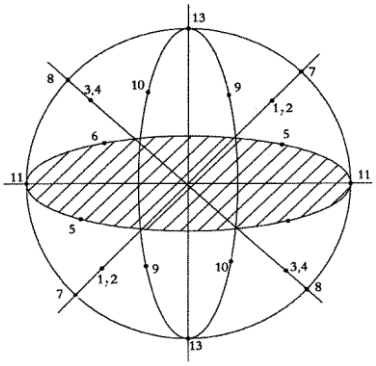

Figure 8. The position of the sphere and the 26 mentioned points.

The Equation of the sub-loading surface $f(\boldsymbol{\sigma})$ is also as follows.

$$f(\boldsymbol{\sigma}) = (\boldsymbol{\sigma}_n) + \frac{2}{3} \times \frac{\tau}{M_{cr}(\sigma_n)} = RF(H) \quad (36)$$

In the above relationship, the parameters σ_n and τ represent the amount of normal and shear stress in each plane.

6. Modelling triaxial tests

In the following research, the modelling of triaxial tests in drained and undrained conditions for four clay samples was done using the unified model and multilaminate theory and its results were compared with laboratory results. In Table 2, the parameters used for the clay samples studied in this research are presented.

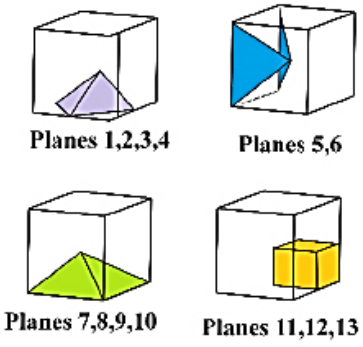

Figure 9. Extension of the 13 planes in the center of the cube.

6.1. Triaxial drained test on Weald clay

The prediction of drained triaxial compressive behavior under constant lateral pressure using the unified model and multilaminate model is presented in Figs. 7 and 8 for Weald clay and kaolinite-silt mixtures. In general, according to the results, the unified model is well able to model the phase transition behavior from elastic to plastic state. Also, the concavity and convexity of stress- axial strain curve and volumetric strain-axial strain curve can be well modeled by the unified model. Laboratory drained triaxial test on Weald clay soil was performed by Skempton & Brown (1961) [26]. The results of the stress-strain diagrams of the above-mentioned model with the results obtained from the laboratory tests are presented in Figure. According to the obtained results, the agreement of the model with the laboratory data is very high. The initial stress state in this test $\sigma_0 = -671$ kPa .

6.2. Triaxial drained test on Kaolinite-silt mixtures

Laboratory drained triaxial test on kaolinite–silt mixtures soil by Stark et al. (1994) has been done [27]. The proposed model provides relatively acceptable results for both stress-axial strain and volumetric strain-axial strain diagrams, and the trend of the graphs follows the trend of the laboratory graphs. The initial stress state in this test is: $\sigma_0 = -1275?$ kPa. It is clear that the unified model has a better prediction than the multilaminate model for stress-axial strain and volumetric strain-axial strain diagrams. The consistency of the results of the unified model with the laboratory data is better (Fig. 11).

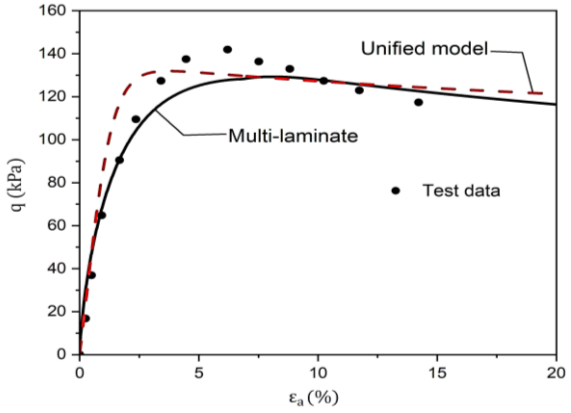

(a) Deviatoric stress- axial strain curve.

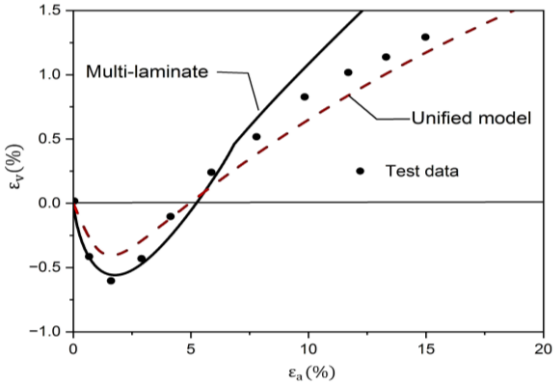

(b) Volumetric strain - axial strain curve.

Figure 10. Comparison of modelling results with laboratory data on Weald clay soil for drained triaxial compression test under constant lateral pressure.

Table 1. Plane numbers, direction cosines, and their weighting coefficients.

Plane NO		1	2	3	4	5	6	7	8	9	10	11	12	13
Normal axis	l_i	$\frac{\sqrt{3}}{3}$	$\frac{\sqrt{3}}{3}$	$-\frac{\sqrt{3}}{3}$	$-\frac{\sqrt{3}}{3}$	$\frac{\sqrt{2}}{2}$	$-\frac{\sqrt{2}}{2}$	$\frac{\sqrt{2}}{2}$	$-\frac{\sqrt{2}}{2}$	0	0	1	0	0
	m_i	$\frac{\sqrt{3}}{3}$	$-\frac{\sqrt{3}}{3}$	$\frac{\sqrt{3}}{3}$	$-\frac{\sqrt{3}}{3}$	$\frac{\sqrt{2}}{2}$	$\frac{\sqrt{2}}{2}$	0	0	$-\frac{\sqrt{2}}{2}$	$\frac{\sqrt{2}}{2}$	0	1	0
	n_i	$\frac{\sqrt{3}}{3}$	$\frac{\sqrt{3}}{3}$	$\frac{\sqrt{3}}{3}$	$\frac{\sqrt{3}}{3}$	0	0	$\frac{\sqrt{2}}{2}$	$\frac{\sqrt{2}}{2}$	$\frac{\sqrt{2}}{2}$	$\frac{\sqrt{2}}{2}$	0	0	1
W_i		$\frac{27}{840}$	$\frac{27}{840}$	$\frac{27}{840}$	$\frac{27}{840}$	$\frac{32}{840}$	$\frac{32}{840}$	$\frac{32}{840}$	$\frac{32}{840}$	$\frac{32}{840}$	$\frac{32}{840}$	$\frac{40}{840}$	$\frac{40}{840}$	$\frac{40}{840}$

Table 2. The parameters of the studied soils.

Parameter		Weald Clay	Kaolinite–Silt	London Clay	Red Clay
Elastic parameters	G(kPa)	6500	18000	12000	2000
	κ	0.002	0.006	0.0063	0.012
Critical state parameters	$M_{cr,c}$	1.2	1.36	1.3	1.20
	$M_{cr,e}$	0.8	1.051	0.82	1.015
	λ	0.045	0.1	0.022	0.035
	ϑ_Γ	1.63	0.63	1.2	2.63
Bounding surface	N	1.5	6.0	6.0	1.30
	R	2.718	2.0	2.25	2.718
Dilatancy (Flow rule)	d_0	1.2	1.2	1.2	1.2
	β	0	0	0	0
	m	0	0	0	0
Hardening	u_0	33	35	70	20
	S_0(kPa)	10	20	10	10

6.3. Triaxial undrained test on London clay

Stress path and stress-strain curves were estimated by the unified model and multilaminate model and their results were compared with the results of laboratory tests. The laboratory results can be well modeled by both models. Undrained triaxial test on London clay soil by Bishop et al. (1965) has been done [28]. According to the results of the laboratory data, they can be better modeled by the unified model (Figure 12).

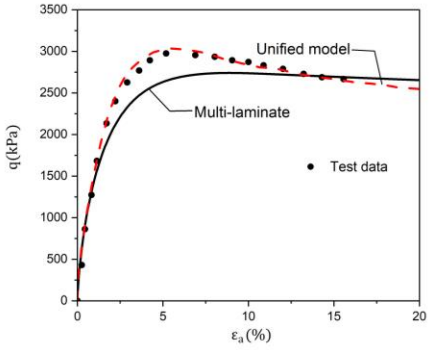

(a) Deviatoric stress- axial strain curve.

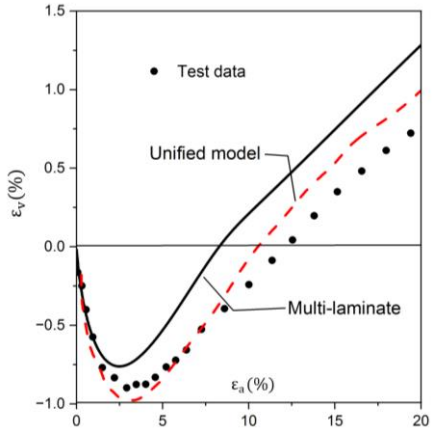

(b) Volumetric strain - axial strain curve.

Figure 11. Comparison of the calculated results from the following models with the test data (after Stark et al., 1994) for the drained triaxial compressive test with constant lateral pressure for kaolinite–silt mixtures.

6.4. Triaxial undrained test on Red clay

Undrained triaxial test on red clay soil was performed by Wesley (1990) [29]. Triaxial tests have been performed under three constant lateral pressures of 50, 100, and 250 kPa. Unlike the multilaminate model, the unified model predicts well the stress-strain diagram and the stress path in accordance with the test data (Figure 13).

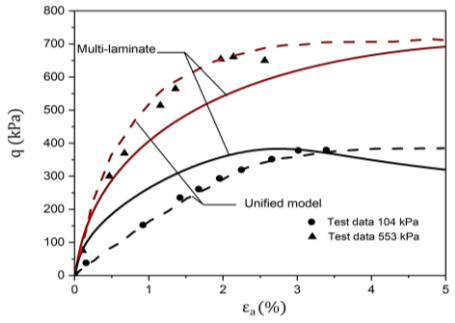

(a). Deviatoric stress- axial strain curve.

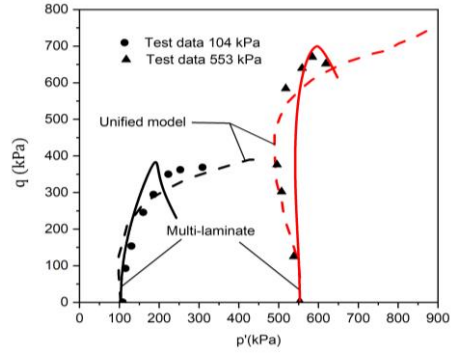

(b). Deviatoric stress - effective stress curve.

Figure 12. Comparison of model results with undrained triaxial compressive test data under constant lateral pressure for Red Clay.

7. Conclusions

In this research, two behavior models, including the unified and multilaminate theory, have been used for soil modelling. The unified behavior model is an elastic-plastic model designed to simulate the behavior of clay and sand under monotonic drained and undrained conditions based on the concept of the bounding surface. This model utilizes the concepts of critical state and state parameter to predict the unified behavior of sand and clay. It also incorporates a general dilatancy rule in its formulation to capture the behavioral characteristics of over consolidated clay and dense sand, including phase transition behavior. Additionally, to predict softening behavior using the bounding surface concept, a new formulation based on the radial mapping rule has been

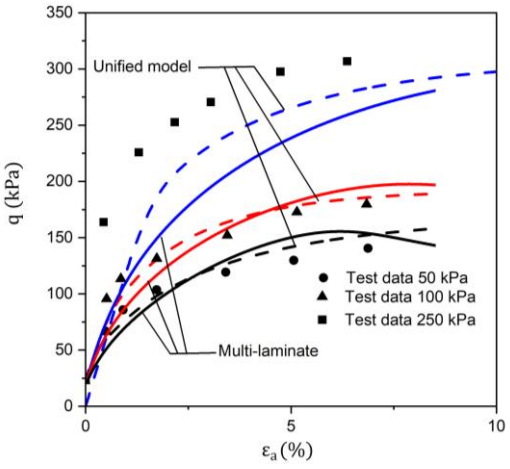

(a) Deviatoric stress- axial strain curve.

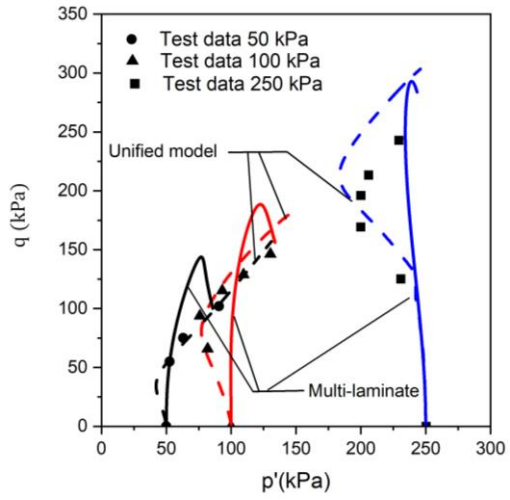

b) Deviatoric stress - effective stress curve.

Figure 13. Comparison of model results with undrained triaxial compressive test data under constant lateral pressure for Red Clay

employed. In addition, the proposed model was implemented using Euler's implicit method based on a return mapping rule. In the multilaminate model, a 13-plane model is used, each of which has elastic-plastic behavior. The behavior of the soil is obtained from the sum of the behavior of these planes. A series of non-classical structural equations has been used in each of the planes separately. This model is able to estimate the soil softening behavior more realistically due to the use of a non-classical plasticity model. In fact, it also takes into account the effect of induced anisotropy. The following results were obtained from modelling four soil samples under monotonic loading with triaxial tests, both in drained and undrained conditions, and compared with reported laboratory data:

- The unified model shows a more acceptable performance in modelling soil behavior under monotonic loading in both drained and undrained conditions.
- The model accurately predicts the behavioral characteristics of clay and sand under monotonic loading, including:
  - Soft behavior from elastic to plastic
  - Softening and hardening behavior
  - Dilatancy
  - Phase transition behavior
- The implicit method based on the return mapping algorithm ensures optimal accuracy and convergence of responses for both large and small strains.

In this paper, the behavior of soils was examined using two unified behavioral models: isotropic (unified model) and anisotropic (multi-laminate). For future studies, combining the unified behavioral model with multi-laminate theory could provide a more effective approach to modelling soil behavior. The results of the developed unified code in the monotonic loading state were validated against laboratory data. Modelling cyclic tests using a hybrid unified model can significantly aid in validating the developed code. Since soils are predominantly anisotropic, incorporating a rotational hardening rule into the unified code enhances the model's capacity to represent anisotropic materials. In this context, the developed code was also validated against the results of triaxial and hollow cylinder tests.

Notation

σ_1: major principal stress
σ_2: intermediate principal stress
σ_3: minor principal stress
p': average effective stress
q: deviatoric stress
ε_1: : major principal strain
ε_2: intermediate principal strain
ε_3: minor principal strain
ε_V: volumetric strains
ε_q: deviatoric strains
$\boldsymbol{\varepsilon}^e$: elastic strain vector
$\boldsymbol{\varepsilon}^p$: plastic strain vector
e: void ratio
e_{cr}: critical void ratio
e_Γ: the critical state void ratio when $p' = 1kPa$
λ_{cr}: slope of the critical state line in the $e - lnp'$ plane
M_{cr}: The slope of the critical state line in q-p' space
t: scalar variable
φ: friction angle
M_c: Slope of the critical state line in compressive loading
M_e: Slope of the critical state line in extensive loading
ψ: state parameter
ϑ: specific volume
ϑ_{cr}: specific volume at the critical state
ϑ_Γ: reference specific volume on the critical state line at a unit confining pressure
λ: the elastoplastic compressibility coefficient
K: bulk modulus
ν: specific volume
κ: elastic compressibility coefficient
μ: Poisson's ratio
γ: size ratio (ratio of subloading surface size to normal yield surface size)
$\boldsymbol{\sigma}$: current stress state
$\boldsymbol{\sigma}_j$: image stress state on the bounding surface
q_j: deviatoric stress corresponding to the image stress state
p'_j: average effective stress corresponding to the image stress state
p'_c: parameter defines the size of the loading surface
p'_{cj}: parameter defines the size of the bounding surface
N: model parameter
R: model parameter
d_0: material parameter
$\bar{\eta}$: stress ratio
β: material parameter
m: material parameter
Q: plastic potential surface
U: parameter controlling the transition behavior from elastic to plastic

$\mathbf{D}^e$: elastic stiffness matrix

σ_n: normal stress

τ: shear stress

References

[1] Roscoe, K. H. (1963). Mechanical behaviour of an idealised 'wet clay'. In *Proceedings of the 2nd European Conference on Soil Mechanics* (pp. 47-54). http://www-civ.eng.cam.ac.uk/geotech_new/people/ans/wetclay.pdf

[2] Roscoe, K. H., Schofield, A., & Thurairajah, A. (1963). Yielding of clays in states wetter than critical. *Geotechnique, 13*(3), 211-240. Doi: https://doi.org/10.1680/GEOT.1963.13.3.211

[3] Pender, M. J. (1978). A model for the behaviour of overconsolidated soil. *Geotechnique, 28*(1), 1-25. Doi: https://doi.org/10.1680/geot.1978.28.1.1

[4] Chen, Y. N., & Yang, Z. X. (2017). A family of improved yield surfaces and their application in modeling of isotropically over-consolidated clays. *Computers and Geotechnics, 90*, 133-143. Doi: https://doi.org/10.1016/j.compgeo.2017.06.007

[5] Roscoe, K., & Burland, J. B. (1968). On the generalized stress-strain behaviour of wet clay. Doi: https://doi.org/10.1016/0022-4898(70)90160-6

[6] Naylor, D. J. (1985). A continuous plasticity version of the critical state model. *International Journal for Numerical Methods in Engineering, 21*(7), 1187-1204. Doi: https://doi.org/10.1002/nme.1620210703

[7] Paston, M., Zienkiewicz, O. C., & Leung, K. H. (1985). Simple model for transient soil loading in earthquake analysis. II. Non-associative models for sands. *International Journal for Numerical and Analytical Methods in Geomechanics, 9*(5). Doi: https://doi.org/10.1002/nag.1610090506

[8] Been, K., & Jefferies, M. G. (1985). A state parameter for sands. *Géotechnique, 35*(2), 99-112. Doi: https://doi.org/10.1680/geot.1985.35.2.99

[9] Nova, R., & Wood, D. M. (1979). A constitutive model for sand in triaxial compression. *International Journal for Numerical and Analytical Methods in Geomechanics, 3*(3), 255-278. Doi: https://doi.org/10.1002/nag.1610030305

[10] Jefferies, M. G. (1993). Nor-Sand: a simple critical state model for sand. *Géotechnique, 43*(1), 91-103. Doi: https://doi.org/10.1680/geot.1993.43.1.91

[11] Wroth, C. P., & Bassett, R. H. (1965). A stress–strain relationship for the shearing behaviour of a sand. *Géotechnique*, 15(1), 32-56. Doi: https://doi.org/10.1680/geot.1965.15.1.32

[12] Jocković, S., & Vukićević, M. (2017). Bounding surface model for overconsolidated clays with new state parameter formulation of hardening rule. *Computers and Geotechnics*, 83, 16-29. Doi: https://doi.org/10.1016/j.compgeo.2016.10.013

[13] Jian, L. I., Chen, S., & Jiang, L. (2016). On implicit integration of the bounding surface model based on swell–shrink rules. *Applied Mathematical Modelling*, 40(19-20), 8671-8684. Doi: https://doi.org/10.1016/j.apm.2016.05.014

[14] Khalili, N., Habte, M. A., & Valliappan, S. (2005). A bounding surface plasticity model for cyclic loading of granular soils. *International Journal for Numerical Methods in Engineering*, 63(14), 1939-1960. Doi: https://doi.org/10.1002/nme.1351

[15] Ling, H. I., & Yang, S. (2006). Unified sand model based on the critical state and generalized plasticity. *Journal of Engineering Mechanics*, 132(12), 1380-1391. Doi: https://doi.org/10.1061/(ASCE)0733-9399(2006)132:12(1380)

[16] Manzari, M. T., & Dafalias, Y. F. (1997). A critical state two-surface plasticity model for sands. *Géotechnique*, 47(2), 255-272. Doi: https://doi.org/10.1680/geot.1997.47.2.255

[17] da Fonseca, A. V., Molina-Gómez, F., Ferreira, C., & Quintero, J. (2023). Modelling the critical state behaviour of granular soils: Application of NorSand constitutive law to TP-Lisbon sand. *Geomechanics and Engineering*, 34(3), 317-328. Doi: https://doi.org/10.12989/gae.2023.34.3.317

[18] Yu, H. S. (1998). CASM: A unified state parameter model for clay and sand. *International Journal for Numerical and Analytical Methods in Geomechanics*, 22(8), 621-653. Doi: https://doi.org/10.1002/(SICI)1096-9853(199808)22:8<621::AID-NAG937>3.0.CO;2-8

[19] Yu, H. S., & Khong, C. D. (2003). Bounding surface formulation of a unified critical state model for clay and sand. In *Deformation Characteristics of Geomaterials*, IS Lyon 2003 (pp. 1111-1118). Doi: https://doi.org/10.1016/j.mechrescom.2006.06.010

[20] Fincato, R., & Tsutsumi, S. (2017). Closest-point projection method for the extended subloading surface model. *Acta Mechanica*, 228, 4213-4233. Doi: https://doi.org/10.1007/s00707-017-1926-0

[21] Hu, C., & Liu, H. (2014). Implicit and explicit integration schemes in the anisotropic bounding surface plasticity model for cyclic behaviours of saturated clay. *Computers and Geotechnics*, 55, 27-41. Doi: https://doi.org/10.1016/j.compgeo.2013.07.012

[22] Rouainia, M., & Muir Wood, D. (2001). Implicit numerical integration for a kinematic hardening soil plasticity model. *International Journal for Numerical and Analytical Methods in Geomechanics*, 25(13), 1305-1325. Doi: https://doi.org/10.1002/nag.179

[23] Manzari, M. T., & Nour, M. A. (1997). On implicit integration of bounding surface plasticity models. *Computers & Structures*, 63(3), 385-395. Doi: https://doi.org/10.1016/S0045-7949(96)00373-2

[24] Moghadam, S. I., Taheri, E., Ahmadi, M., & Ghoreishian Amiri, S. A. (2022). Unified bounding surface model for monotonic and cyclic behaviour of clay and sand. *Acta Geotechnica*, 17(10), 4359-4375. Doi: https://doi.org/10.1007/s11440-022-01521-9

[25] Li, X. S., & Dafalias, Y. F. (2000). Dilatancy for cohesionless soils. *Géotechnique*, 50(4), 449-460. Doi: https://doi.org/10.1680/geot.2000.50.4.449

[26] Skempton, A. W., & Brown, J. D. (1961). A landslide in boulder clay at Selset, Yorkshire. *Geotechnique*, 11(4), 280-293. Doi: https://doi.org/10.1680/sposm.02050.0016

[27] Stark, T. D., Ebeling, R. M., & Vettel, J. J. (1994). Hyperbolic stress-strain parameters for silts. *Journal of Geotechnical Engineering*, 120(2), 420-441. Doi: https://doi.org/10.1061/(ASCE)0733-9410(1994)120:2(420)

[28] Bishop, A. W., Webb, D. L., & Lewin, P. I. (1965). Undisturbed samples of London Clay from the Ashford Common shaft: strength–effective stress relationships. *Geotechnique*, 15(1), 1-31. Doi: https://doi.org/10.1680/geot.1965.15.1.1

[29] Wesley, L. D. (1990). Influence of structure and composition on residual soils. *Journal of geotechnical engineering, 116*(4), 589-603. Doi: https://doi.org/10.1061/(ASCE)0733-9410(1990)116:4(589)

[30] Jeong, S., Ko, J., Song, S., & Kim, J. (2024). The behaviors of a Korean weathered soil under monotonic loadings. *Geomechanics and Engineering*, 38(2), 157-164. Doi: . https://doi.org/10.12989/gae.2024.38.2.157

[31] Bella, G., & Musso, G. (2024). Liquefaction susceptibility of silty tailings under monotonic triaxial tests in nearly saturated conditions. *Geomechanics and Engineering: An International Journal*, 36(3), 247-258. Doi: https://doi.org/10.12989/gae.2024.36.3.247

[32] Yu, H. S. (2007). *Plasticity and Geotechnics* (Vol. 13). Springer Science & Business Media. Doi: https://doi.org/10.1007/978-0-387-33599-5

[33] Schofield, A. N., & Wroth, P. (1968). *Critical state soil mechanics* (Vol. 310). London: McGraw-Hill. Doi: http://www-civ.eng.cam.ac.uk/geotech_new/publications/schofield_wroth_1968.pdf

[34] Yu, H. S., Khong, C., & Wang, J. (2007). A unified plasticity model for cyclic behaviour of clay and sand. *Mechanics Research Communications*, 34(2), 97-114. Doi: . https://doi.org/10.1016/j.mechrescom.2006.06.010

[35] Hashiguchi, K. (2017). *Foundations of elastoplasticity: subloading surface model*. New York: Springer. Doi: https://doi.org/10.1007/978-3-030-93138-4

[36] Dafalias, Y. F., & Popov, E. P. (1975). A model of nonlinearly hardening materials for complex loading. *Acta Mechanica*, 21(3), 173-192. Doi: https://doi.org/10.1007/BF01181053

[37] Hashiguchi, K., Ueno, M., & Chen, Z. P. (1996). Elastoplastic constitutive equation of soils based on the concepts of subloading surface and rotational hardening. *Doboku Gakkai Ronbunshu*, 1996(547), 127-144. Doi: https://doi.org/10.1002/(SICI)10969853(199803)22:3<197::AID-NAG914>3.0.CO;2-T

[38] Hashiguchi, K. (1989). Subloading surface model in unconventional plasticity. *International Journal of Solids and Structures*, 25(8), 917-945. Doi: https://doi.org/10.1016/0020-7683(89)90038-3

[39] Dafalias, Y. F. (1981). The concept and application of the bounding surface in plasticity theory. In *Physical Non-Linearities in Structural Analysis: Symposium Senlis, France May 27–30, 1980* (pp. 56-63). Berlin, Heidelberg: Springer Berlin Heidelberg. Doi: https://doi.org/10.1007/978-3-642-81582-9_9

[40] Hu, C., & Liu, H. (2015). A new bounding-surface plasticity model for cyclic behaviors of saturated clay. *Communications in Nonlinear Science and Numerical Simulation*, 22(1-3), 101-119. Doi: https://doi.org/10.1016/j.cnsns.2014.10.023

[41] Dafalias, Y. F., & Herrmann, L. R. (1986). Bounding surface plasticity. II: Application to isotropic cohesive soils. *Journal of Engineering Mechanics*, 112(12), 1263-1291. Doi: https://doi.org/10.1061/(ASCE)0733-9399(1986)112:12(1263)

[42] Lu, Y., Zhu, W. X., Ye, G. L., & Zhang, F. (2021). A unified constitutive model for cemented/non-cemented soils under monotonic and cyclic loading. *Acta Geotechnica*, 16(1), 1-19. Doi: https://doi.org/10.1007/s11440-021-01348-w

[43] Wang, R., Cao, W., Xue, L., & Zhang, J. M. (2021). An anisotropic plasticity model incorporating fabric evolution for monotonic and cyclic behavior of sand. *Acta Geotechnica*, 16(1), 43–65. Doi: https://doi.org/10.1007/s11440-020-00984-y

[44] Rezania, M., & Dejaloud, H. (2021). BS-CLAY1: Anisotropic bounding surface constitutive model for natural clays. *Computers and Geotechnics*, 135, 104099. Doi: https://doi.org/10.1016/j.compgeo.2021.104099

[45] Rezania, M., Dejaloud, H. (2022). A bounding surface constitutive model with a moving projection centre for highly overconsolidated clays.

[46] Gao, Z., Zhao, J., & Yin, Z. Y. (2017). Dilatancy relation for overconsolidated clay. *International Journal of Geomechanics*, 17(5), 06016035. Doi: https://doi.org/10.1061/(ASCE)GM.1943-5622.0000793

[47] Verbrugge, J. C., & Schroeder, C. (2018). Geotechnical Correlations for Soils and Rocks. John Wiley & Sons. Doi:10.1002/9781119482819

[48] Schuller, H., & Schweiger, H. F. (2002). Application of a multilaminate model to simulation of shear band formation in NATM-tunnelling. *Computers and Geotechnics*, 29(7), 501-524. Doi: https://doi.org/10.1016/S0266-352X(02)00013-7

[49] Dashti, H., Sadrnejad, S. A., & Ganjian, N. (2017). Modification of a constitutive model in the framework of a multilaminate method for post-liquefaction sand. *Latin American Journal of Solids and Structures*, 14, 1569-1593. Doi: https://doi.org/10.1590/1679-78253841

[50] Dashti, H., Sadrnejad, S. A., & Ganjian, N. (2019). A novel semi-micro multilaminate elasto-plastic model for the liquefaction of sand. *Soil Dynamics and Earthquake Engineering*, 124, 121-135. Doi: https://doi.org/10.1016/j.soildyn.2019.05.031

[51] Sadrnejad, S. A., & Hoseinzadeh, M. R. (2019). Multi-laminate rate-dependent modelling of static and dynamic concrete behaviors through damage formulation. *Scientia Iranica*, 26(3), 1194-1205. Doi: 20.1001.1.10263098.2019.26.3.9.2

[52] Peyman, F., & Sadrnejad, S. A. (2019). Numerical Analysis of Sand Behavior based on Modified Multi-laminate Model. *International Journal of New Technology and Research*, 2(8), 263445.

[53] Sadrnejad, S., & Ghoreyshian, A. S. (2010). A simple unconventional plasticity model within the multilaminate framework. http://ijce.iust.ac.ir/article-1-456-en.html

[54] Ghoreishian Amiri, S. A. (2014). Application of the multi-laminate sub-loading surface model in the simulation of a pipe-jacking operation. *Numerical Methods in Civil Engineering*, 1(2), 41-47. Doi: https://doi.org/10.29252/NMCE.1.2.41